39th AIAA Fluid Dynamics Conference
22 - 25 June 2009, San Antonio, Texas

AIAA 2009-4054

Hypersonic Wind-Tunnel Measurements of Boundary-Layer Pressure Fluctuations

Katya M. Casper*
School of Aeronautics and Astronautics, Purdue University, West Lafayette, IN 47907-1282
Sandia National Laboratories, Albuquerque, NM 87185

Steven J. Beresh†, John F. Henfling‡, Russell W. Spillers§, and Brian Pruett¶
Sandia National Laboratories, Albuquerque, NM 87185

Steven P. Schneider‖
School of Aeronautics and Astronautics, Purdue University, West Lafayette, IN 47907-1282

During atmospheric reentry, hypersonic vehicles are subjected to high levels of boundary-layer pressure fluctuations. To improve understanding and prediction of these fluctuations, measurements of surface pressure fluctuations on a 7° sharp cone were conducted in Sandia's Hypersonic Wind Tunnel under noisy flow and in Purdue University's Boeing/AFOSR Mach-6 Quiet Tunnel under noisy and quiet flow. Fluctuations under laminar boundary layers reflected tunnel noise levels. Laminar boundary-layer measurements under quiet flow were an order of magnitude lower than under noisy flow. Transition on the model only occurred under noisy flow, and fluctuations peaked during transition. The transition location, marked by the peak, was predicted using tunnel noise parameters (Pate's correlation). Turbulent boundary-layer fluctuations were lower than transitional fluctuations and also reflected tunnel noise levels. Measurements of second-mode waves showed the waves started to grow under a laminar boundary layer, saturated, and then broke down near the peak in transitional pressure fluctuations.

Nomenclature

δ^*	boundary-layer displacement thickness	P_0	tunnel stagnation pressure
ϕ	cone azimuthal angle	P_{02}	stagnation pressure behind normal shock
τ_w	nozzle wall shear stress	$\tilde{P}_{02}$	root-mean-square stagnation pressure behind normal shock
c	tunnel test section circumference		
$\overline{c}$	aerodynamic-noise-transition correlation size parameter	$\tilde{p}$	root-mean-square pressure
		p_e	boundary-layer edge pressure
c_1	test section circumference of a 0.305×0.305 m tunnel	q_e	dynamic pressure at boundary-layer edge
		Re/m	freestream unit Reynolds number
$C_{F_{II}}$	mean turbulent skin-friction coefficient calculated using method of Van-Driest II	Re_{t_δ}	transition Reynolds number based on boundary-layer edge conditions
M	freestream Mach number	T_0	tunnel stagnation temperature
M_e	Mach number at boundary-layer edge	x	axial model coordinate measured from nose

*Research Assistant and Sandia Graduate Intern, Student Member AIAA, kcasper@purdue.edu, (765) 494-3348
†Principal Member of the Technical Staff, Engineering Sciences Center, Associate Fellow AIAA
‡Distinguished Technologist, Member AIAA
§Senior Technologist
¶Technologist
‖Professor, Associate Fellow AIAA

Sandia is a multiprogram laboratory operated by Sandia Corporation, a Lockheed Martin Company, for the United States Department of Energy's National Nuclear Security Administration under contract DE-AC04-94AL85000.

I. Introduction

Hypersonic reentry vehicles are subjected to high levels of fluctuating pressures. These intense fluctuations can cause vibration of internal components and can lead to structural fatigue. There is a need to predict the magnitude and location of the pressure fluctuations to better design reentry vehicles. Current designs often use overly conservative estimates of the fluctuations which can lead to heavier vehicles and degraded flight performance. Some correlations exist for the magnitude of laminar, transitional, and turbulent pressure fluctuations, but these were derived primarily using either incompressible data or conventional (noisy flow) hypersonic wind-tunnel tests.[1–8]

Extensive work was done to study freestream noise in wind tunnels, particularly during the 1960's and 1970's. Laufer[9] discovered that although the dominant source of tunnel disturbances at low speeds was freestream vorticity disturbances, at Mach numbers higher than 3, the acoustic noise radiated from turbulent boundary layers on the walls was the dominant disturbance. This noise increases with increasing Mach number. The noise level in conventional hypersonic tunnels, defined as the root-mean-square (rms) Pitot pressure over the mean Pitot pressure, is typically near 1% and sometimes as high as 2–5%.[10] Noise levels can be even higher if the wall boundary layer is transitioning. These conventional tunnel noise levels are an order of magnitude higher than flight.[11,12] High noise levels have also been shown to cause transition on models much earlier than in flight.[11–13] To address this issue, quiet tunnels have been developed to better simulate flight noise levels.[14,15] Quiet tunnels maintain laminar boundary layers on the tunnel wall to avoid the noise radiation from turbulent boundary layers. However, they are still not common as it is difficult and costly to maintain laminar boundary layers on the nozzle wall for long distances and high Reynolds number. Most research is still done in conventional tunnels making it important to understand the effect of noise on the results.

Early work suggested that pressure fluctuations measured on the surface of a sharp cone under a laminar boundary layer were equal to the freestream pressure fluctuations.[16–19] Stainback et al.[17] conducted experiments that suggested that the freestream tunnel noise was not attenuated through the cone shock. This meant that the acoustic disturbances in the tunnel freestream entered the model laminar boundary layer and remained constant. A series of papers broke with this understanding in the mid 1970's.[10] Beckwith,[14] Kendall,[20] and Pate[21] showed experimental results that freestream noise could be amplified within the laminar boundary layer. This phenomenon was consistent with Mack's[22] forcing theory, developed near the same time. The theory explained the interaction of low-frequency freestream noise components with a laminar boundary layer and allowed for the amplification of freestream noise without an instability, sometimes by factors as high as 5–20. Schopper[23] complemented Mack's forcing theory by studying the interaction of the higher-frequency freestream noise with a laminar boundary layer. The refraction and focusing of weak shocks in the upper half of the boundary layer (termed the caustic layer) was shown to increase disturbances by factors of 2–6. High-frequency components were low-pass filtered by the caustic layer. Schopper could not find experimental confirmation of the caustic layer, and it is not known if this theory was ever experimentally verified. The question of whether the freestream noise is amplified in the laminar boundary layer as described by either Mack's or Schopper's theories remains unanswered.

Another proposed explanation for observed laminar boundary layer fluctuations higher than the freestream noise is that the edge of the boundary layer can be transitional/turbulent while the surface remains laminar. Disturbances spread to the wall at a constant angle.[24] Surface pressure measurements upstream of the surface transition location might be influenced by transition or turbulence in the outer portions of the boundary layer.[3]

Wind-tunnel tests at fixed freestream conditions have shown that transitional pressure fluctuations can be more severe than turbulent pressure fluctuations, making transitional fluctuations of primary interest for this work. The surface pressure fluctuations show a distinct peak near the end of transition.[3,25–28] That peak has been shown to correspond to the point of maximum heat transfer often used to define the end of transition.[3,28] In this paper, transition will be defined in this manner; the peak pressure fluctuations occur near the end of transition. However, Owen and Horstman[29] and Martellucci[3] point out that there is still a region of non-similar flow after the peak in heat transfer that should still be considered part of the transitional region, though it is traditionally defined as turbulent.

In order to improve prediction of hypersonic pressure fluctuations, experiments were conducted on a 7° sharp cone at zero angle of attack in two hypersonic tunnels under conventional and quiet noise levels. Surface-mounted pressure sensors were used to measure the surface pressure fluctuations. Experiments under noisy flow were conducted in the Sandia National Laboratories Hypersonic Wind Tunnel (HWT) at Mach

5 and 8 and in the Boeing/AFOSR Mach-6 Quiet Tunnel (BAM6QT) at Purdue University. Measurements under quiet flow were also conducted in the BAM6QT for comparison to noisy-flow measurements and flight data. The BAM6QT is the only operational hypersonic quiet tunnel in the world. It features low noise of about 0.05%, which is similar to flight and an order of magnitude lower than conventional tunnels.[30]

II. Wind-Tunnel Facilities

A. Sandia Hypersonic Wind Tunnel

The Sandia Hypersonic Wind Tunnel (HWT) is a blowdown-to-vacuum facility (Figure 1). Interchangeable nozzle and heater sections allow the tunnel to be run at Mach 5, 8, or 14. Mach 5 tests use air as the driver gas while Mach 8 and Mach 14 run with nitrogen. Tests were only conducted at Mach 5 and 8 for this study. HWT-5 has a P_0 range of 345–1380 kPa and a T_0 range of 330–890 K, giving a Re/m range of $3.3–26 \times 10^6$. The test-section diameter is 0.459 m at the nozzle exit, and the nozzle is 3.251 m long, from the throat to the test-section end. HWT-8 has a P_0 range of 1720–6890 kPa, T_0 range of 500–890 K, and Re/m can be varied from $3.3–20 \times 10^6$. The Mach 8 test-section diameter is 0.359 m at the nozzle exit, and the nozzle is 2.807 m long. Run times were typically 15–30 s for these tests.

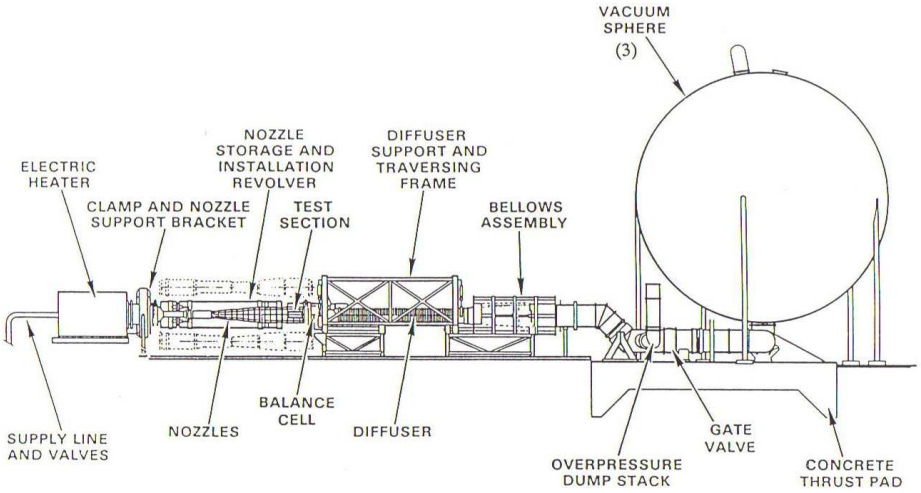

Figure 1. Sandia Hypersonic Wind Tunnel

B. Boeing/AFOSR Mach-6 Quiet Tunnel

The BAM6QT (Figure 2) can be operated as a conventional noisy tunnel or as a quiet tunnel. The tunnel is a Ludwieg tube, a long tube with a converging-diverging nozzle on the end. The flow passes from the driver tube, through the test section, diffuser, a second throat, and finally to the vacuum tank. Flow is initiated by bursting a double diaphragm that is located downstream of the diffuser. When the flow begins, an expansion wave travels upstream and then reflects between the upstream end of the driver tube and the contraction. The total pressure and temperature drop with each reflection cycle (every 200 ms) until the tunnel unstarts. Run times of 3–5 s are typical at present. The tunnel uses air as the test gas and operates with an initial P_0 of 34–2070 kPa and an initial T_0 of 430 K, giving a Re/m range of $0.4–18.3 \times 10^6$. The current maximum quiet pressure (P_0) is 1130 kPa which corresponds to $Re/m = 10.5 \times 10^6$. The test-section diameter is 0.241 m at the nozzle exit, and the nozzle is 2.590 m long.

It is difficult to obtain quiet flow in a hypersonic tunnel. The nozzle is polished to a mirror finish to avoid roughness-induced transition. The contraction boundary layer is also removed by bleed slots at the throat, for quiet runs. A new laminar boundary layer begins just upstream of the nozzle throat and is maintained through the test section. The air is filtered to remove dust or other particles above 0.01-microns that may damage the nozzle or trip the boundary layer. More details about the development of the BAM6QT can be found in Reference 15.

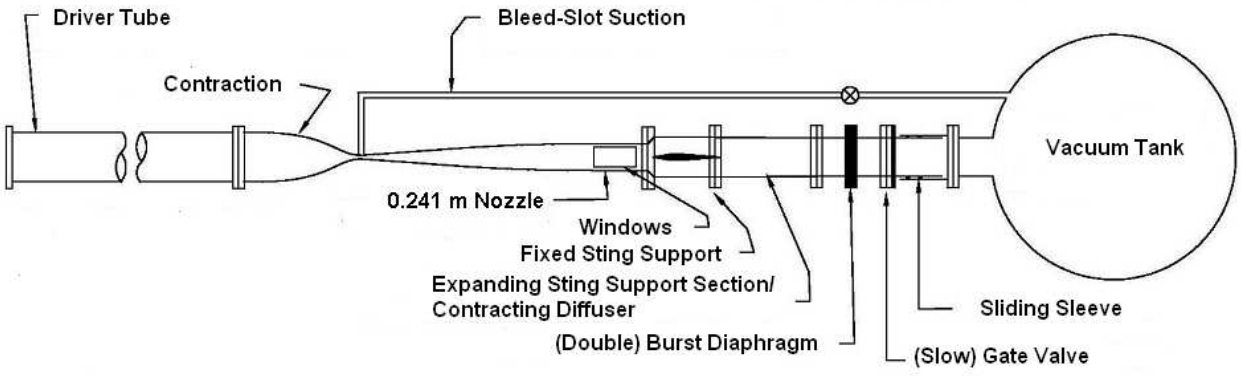

Figure 2. Boeing/AFOSR Mach-6 Quiet Tunnel

III. Pressure Fluctuation Cone

The Pressure Fluctuation Cone was used for all wind-tunnel tests. The model is a 7° half-angle stainless-steel cone. It has many interchangeable parts that allow flexibility for use in a variety of tunnels and experiments (Figure 3). The cone has four sections. The first section is the nosetip. Two sharp nosetips with maximum 0.05 mm radius were tested. Pictures of these nosetips under a microscope can be found in Reference 31. The second section is a blank cone forebody section. It is interchangeable with a glow-perturber section that will allow controlled disturbances to be introduced into the boundary layer in future experiments. Only the blank section of the cone was used for these experiments. The third and fourth sections of the cone are designed to hold the instrumentation. The model can be run as a 0.102-m base-diameter cone using the third section only, or the fourth section can be added to increase the cone base diameter to 0.127 m. These correspond to model lengths of 0.414 m and 0.517 m, respectively. Both sections split in half axially to allow access to the inside of the cone for instrumentation. One side of the cone is a solid section without instrumentation inserts. The other half of the cone can hold a series of sensor inserts. Figure 4 shows the insert positions and Table 1 lists the sensor locations.

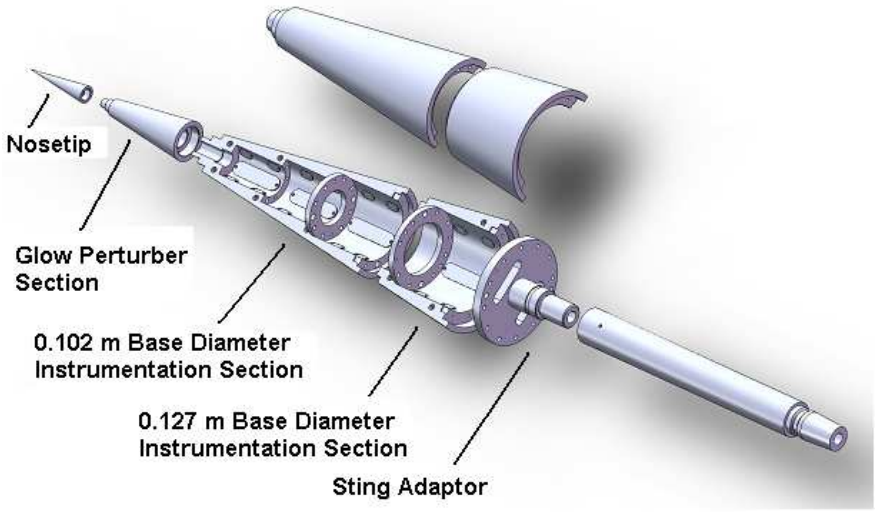

Figure 3. Exploded view of Pressure Fluctuation Cone

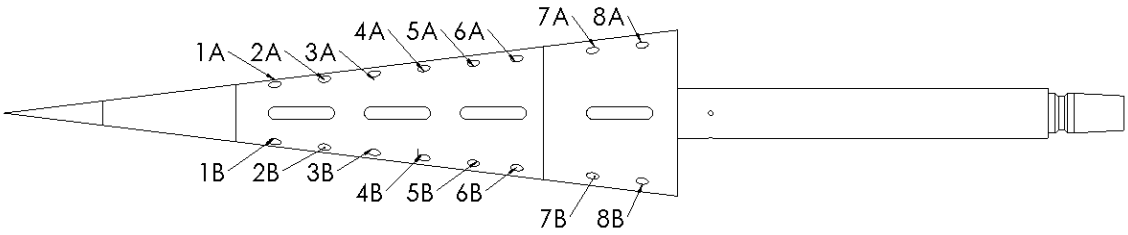

Figure 4. Insert locations for individual sensors

Table 1. Individual sensor locations

Location	x (m)	ϕ (degrees)	Location	x (m)	ϕ (degrees)
1A	0.208	0	1B	0.208	120
2A	0.246	0	2B	0.246	120
3A	0.284	0	3B	0.284	120
4A	0.322	0	4B	0.322	120
5A	0.360	0	5B	0.360	120
6A	0.398	0	6B	0.398	120
7A	0.452	0	7B	0.452	120
8A	0.490	0	8B	0.490	120

IV. Instrumentation and Data Acquisition

A. Instrumentation

Three types of pressure transducers were used in the tests. Kulite Mic-062 and XCQ-062-15A sensors were used for frequency measurements between 0 and 50 kHz. Measurements between 11 kHz and 1 MHz were made with PCB132A31 sensors. A summary of pressure transducer specifications is given in Table 2.

Table 2. Pressure transducer comparison

Sensor	Measurement Range (kPa)	Sensitivity (mV/Pa)	Resonance Frequency (kHz)	Low Frequency Cutoff (kHz)	Diameter (mm)
Mic-062	± 7	0.207	125	0	1.59
XCQ-062-15A	0–103	0.040	225	0	1.59
PCB132A31	0–345	0.020	> 1000	11	3.18

Kulite pressure transducers use silicon diaphragms as the basic sensing mechanisms. Each diaphragm contains a fully active four-arm Wheatstone bridge. The Kulites have screens to protect the diaphragms from damage. Two types of screens were used. The A-screen (Figure 5(a)) has a large central hole. This screen offers only a small amount of diaphragm protection, but the sensor has a flatter frequency response. The sensitive area of the A-screen sensor is the hole size (0.81 mm^2). The B-screen (Figure 5(b)) has a ring of eight holes around the periphery of a solid screen which offers better diaphragm protection than the A-screen. However, the frequency response rolls off at a lower frequency than for the A-screens.

Both Mic-062 A-screen and B-screen sensors were tested. The microphones measure the pressure differential across a diaphragm, up to ± 7 kPa. The back side of the diaphragm has a pressure reference tube that is approximately 0.05 m long. This tube was bent 90 degrees to fit inside the model and left open to the plenum inside of the model. The plenum gives an approximately steady reference pressure, and high frequency components of this pressure are filtered by the long reference tube. The repeatability of the sensors is approximately 0.1% of the full scale, or 7 Pa.

The XCQ-062-15A sensors are mechanically stopped above 103 kPa to prevent damage to the diaphragms at the high BAM6QT pre-run pressures. Because of their larger measurement range, the sensors are less sensitive than the Mic-062's. However, they have a higher nominal resonant frequency of 225 kHz. The repeatability of the sensors is also approximately 0.1% of the full scale, or 0.1 kPa. Only B-screen XCQ-062's were used in this work, but tests of A-screen sensors are planned.

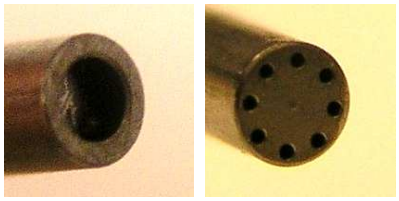

(a) (b)

Figure 5. Kulite screen types (a) A-screen; (b) B-screen

The PCB132A31 is a very high frequency piezoelectric time-of-arrival sensor with a sensor resolution of approximately 7 Pa. Because the resonance frequency of the PCB132's is above 1 MHz, the sensors can measure high-frequency instabilities leading to transition in hypersonic flows.[32,33] Measurements of these instabilities have typically been made by hot wires.[20,34–39] However, hot-wire measurements in hypersonic flow are difficult, and the sensors frequently break. The PCB132's are rugged and can withstand high levels of dynamic pressures without breaking. They allow a study of instability breakdown to transition, and are useful indicators of transition on the model. However, the sensors have not yet been accurately calibrated for this purpose. The repeatability of the sensors is also not specified by the manufacturer. In addition, the sensors have spatial resolution problems for measuring such high-frequency instabilities. Second-mode waves have a wavelength of approximately twice the boundary-layer thickness (approximately 1–3 mm for this work). The PCB132 diameter (3.18 mm) is larger than half of the instability wavelength. Planned dynamic calibrations of the sensors should better define their behavior and limitations.

B. Data Acquisition

The data acquisition systems at each facility are different but provide similar high-speed sampling and anti-aliasing over many channels.

1. Sandia Hypersonic Wind Tunnel

Kulite sensors need an excitation voltage for operation. A 10 V excitation is applied using an Endevco Model 136 DC Amplifier. The amplifier was also used to supply a gain of 100 for Kulite signal output. A Krohn-Hite Model 3384 Tunable Active Filter was used as a 200 kHz anti-aliasing low-pass Bessel filter for the Kulites. The filter has eight poles and provides 48 dB attenuation per octave. The Kulite sampling frequency was 1 MHz. The PCB132 sensors all run through a PCB 482A22 signal conditioner that provides constant-current excitation to the built-in sensor amplifier. The output from the signal conditioner is fed through a Krohn-Hite Model 3944 Filter with a 1 MHz low-pass anti-aliasing Bessel filter. This filter has four poles and offers 24 dB of attenuation per octave. The sampling frequency for the PCB132 sensors was 2.5 MHz. Data is acquired using a National Instruments PXI-1042 chassis with 14-bit PXI-6133 modules (10 MHz bandwidth) for data acquisition. A data sample of 0.75 s was acquired during the constant-condition portion of each wind-tunnel run.

2. Boeing/AFOSR Mach-6 Quiet Tunnel

The signal from the Kulite pressure transducers is processed by custom-built electronics, which also supply a 10 V excitation. The output signal is amplified by a gain of 100 with an INA103 instrumentation amplifier chip to give the DC signal. As in HWT, the output from the PCB sensors is run through a PCB 482A22 signal conditioner.

Two Tektronix DPO7054 and one Tektronix TDS7104 Digital Phosphor Oscilloscopes are used for data acquisition in the BAM6QT. The oscilloscopes have built-in digital filtering. Separate anti-aliasing filters are not required. The DPO7054 has a system bandwidth of 500 MHz and an 8-bit vertical resolution. The resolution can be increased to over 11-bit in Hi-Res mode. Hi-Res mode is used to increase the vertical resolution and reduce random noise. The oscilloscopes average real-time at the maximum sampling rate and then save data at the specified sampling rate. The TDS7104 has similar capabilities, but less memory. Five

seconds of data were recorded for each run. The sampling rate was 500 kHz for the Kulites and 5 MHz for the PCB132's.

V. Experimental Results

A. Sensor Comparison

Sensor comparisons were made with two sensors spaced 120 degrees apart at the same axial location. These comparisons were conducted under a laminar boundary layer to reduce any effect of flow nonuniformities that might arise from asymmetric transition on the cone. Figure 6 shows a comparison between flush-mounted Kulites. The red lines compare two Mic-062 A-screen sensors at x = 0.322 m. The power spectral density (PSD) from the two sensors agree very well, showing that the laminar flow over the cone is fairly axisymmetric. The blue lines show a Mic-062 A-screen and a Mic-062 B-screen at x = 0.398 m. Even though this is the same run, the B-screen sensor rolls off significantly faster than the A-screen sensor. As a result, the B-screen gives a much lower rms pressure than the A-screen. The green lines show the same results when comparing a Mic-062 A-screen and an XCQ-062 B-screen at x = 0.452 m. Again, the XCQ-062 B-screen sensor rolls off significantly faster than the Mic-062 A-screen sensor and gives a much lower rms pressure. Similar results were obtained in the BAM6QT and in HWT-8.[31] Additional tests with each type of sensor placed at the same location on the cone for repeat runs confirmed the same results.

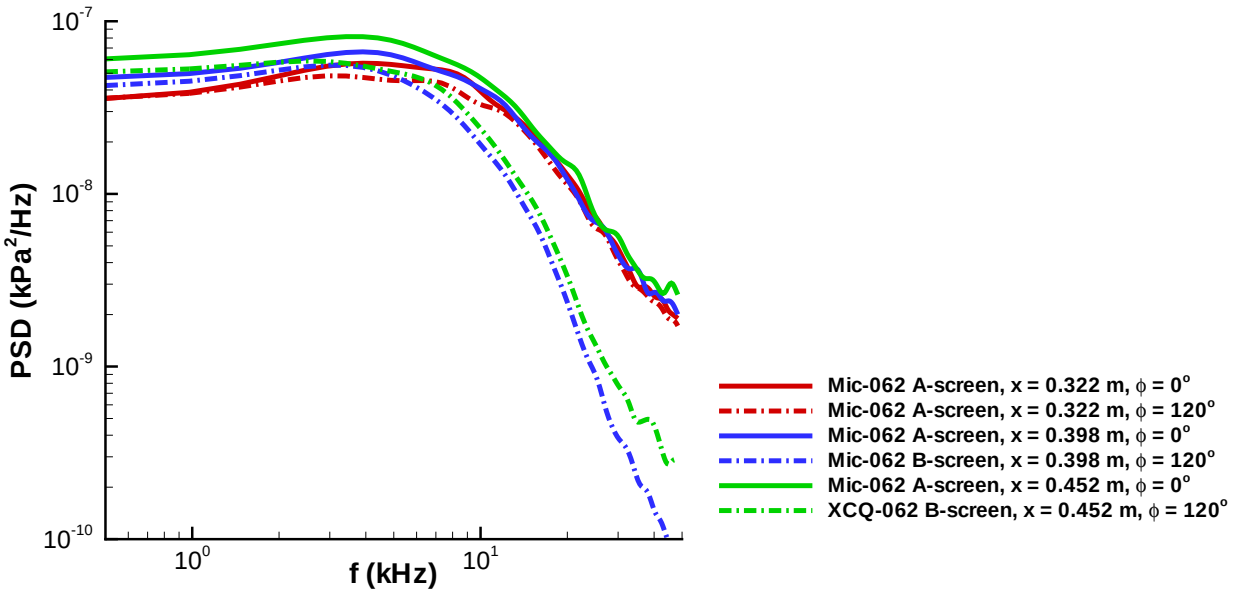

Figure 6. Kulite sensors 120 degrees apart on sharp cone under laminar flow (HWT-5, $Re/m = 4.6 \times 10^6$)

B. Extension of Kulite Spectra to Higher Frequencies using PCB132 sensors

The Mic-062 A-screens seem to provide the best dynamic characteristics among the different Kulites. However, one possibility for the difference in the frequency response of the A and B-screens are cavity effects. The Mic-062 A-screens have large cavities exposed to the flow whereas the B-screens have much smaller holes. The PCB132 sensor offers an independent verification of the Kulite pressure sensors. The PCB132's have a frequency response that overlaps with the Kulites between approximately 11 and 50 kHz. The PCB132's also have a sealed surface so any screen or cavity effects are avoided.

Figure 7 shows a Mic-062 A-screen and a PCB132 spaced 120 degrees apart on the cone at x = 0.360 m. At the lowest Re/m when the boundary layer is laminar at both sensors locations, the PCB132 agrees well with the Mic-062 between 11 and 50 kHz. A small second-mode wave can be seen in the PCB132 spectrum near 180 kHz at $Re/m = 2.9 \times 10^6$. At higher unit Reynolds numbers, the cone boundary layer is beginning to transition near the sensor locations. A larger second-mode wave near 200 kHz as well as a harmonic of

the instability near 400 kHz are present at $Re/m = 5.0 \times 10^6$. The PCB132's also show many noise spikes. It is unclear why the sensors are so sensitive to electrical noise, but the wider bandwidth of the second-mode waves distinguishes them from the narrow noise spikes.

At even higher Re/m, the second-mode waves break down, and the sensors are under a transitional or turbulent boundary layer. In these latter two cases, the two sensors no longer agree; the PCB132's have elevated spectra throughout the 11–50 kHz overlap between the sensors. It is unclear why this happens. Perhaps transition is asymmetric over the cone and the two sensors are measuring a different part of the transitional region. In fact, Mic-062 A-screens spaced 120 degrees apart on the cone do not agree as well as under laminar flow. The PCB132 sensors were designed as time-of-arrival sensors and have not yet been dynamically calibrated. These two types of sensors also have different sensitive areas. Perhaps this discrepancy stems from a nonlinear response, a spatial resolution issue, or from something not yet understood about the sensors. More work is needed to investigate this discrepancy including dynamic sensor calibrations. Similar results were obtained in HWT-5 and HWT-8.[31]

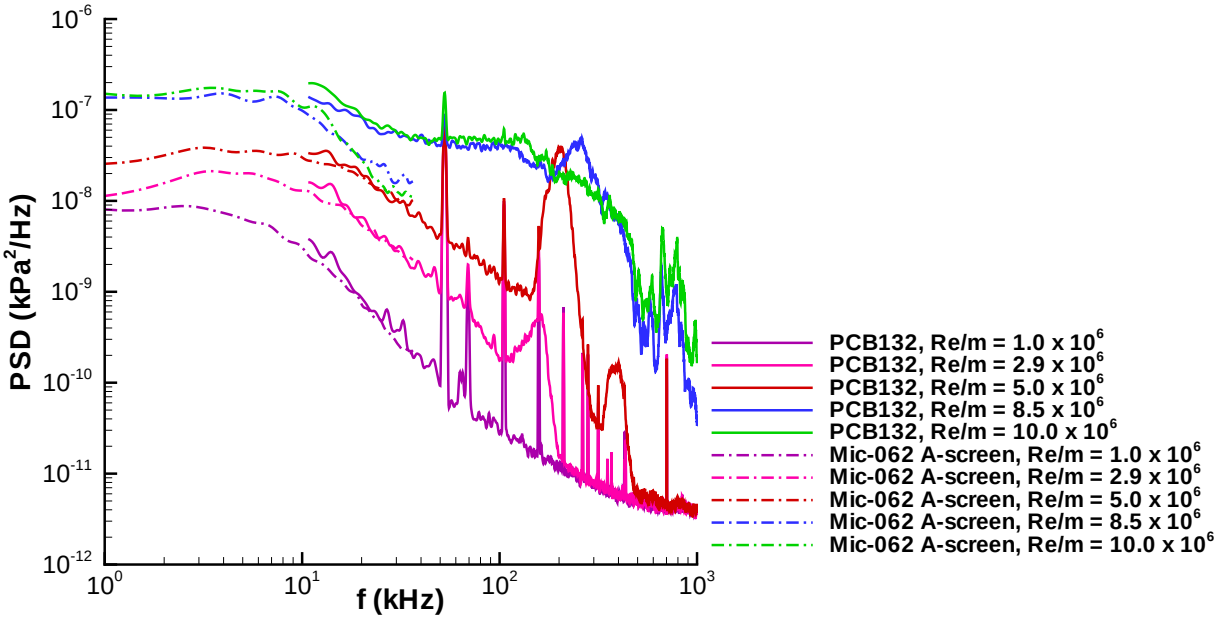

Figure 7. Extension of Mic-062 A-screen spectra with a PCB132 120 degrees apart at x = 0.346 m (BAM6QT, noisy flow)

C. Pressure Fluctuations Along Cone

Pressure fluctuations were measured with a series of eight Mic-062 A-screen sensors along row A of the cone. The sensor at position 4A was broken for tests in HWT-5 and 8. Data from the sensor 120 degrees apart at position 4B were used instead. The B row of sensors measured slightly lower fluctuations than the A row for HWT-5 tests and slightly higher fluctuations for HWT-8 tests.

RMS pressure fluctuations are calculated from the power spectral density between 0 and 50 kHz. Run conditions and normalization values are given in Reference 31. Keye's law was used to calculate viscosity[40] because Sutherland's law is not as accurate at the low freestream temperatures in the tunnels (below 111 K). Real gas effects were neglected. Edge pressure (p_e) and edge dynamic pressure (q_e) were calculated using the Taylor-Maccoll solution for a sharp cone. The nozzle wall shear stress (τ_w) was computed using the method of Van-Driest-II.

1. HWT-5

Figure 8 shows the unnormalized pressure fluctuations along the cone in HWT-5 for increasing Re/m. For the lowest Re/m (marked by squares), the pressure fluctuations remain approximately constant along the cone. The cone boundary layer remains laminar in these cases. At higher Re/m, a peak can be seen in the

pressure fluctuations. This peak occurs near the end of transition.[3,25–28] As Re/m increases further, the peak fluctuations move forward on the cone, showing the upstream movement of transition. At the highest Re/m (marked by triangles), the flow is late transitional or turbulent over the rear of the cone.

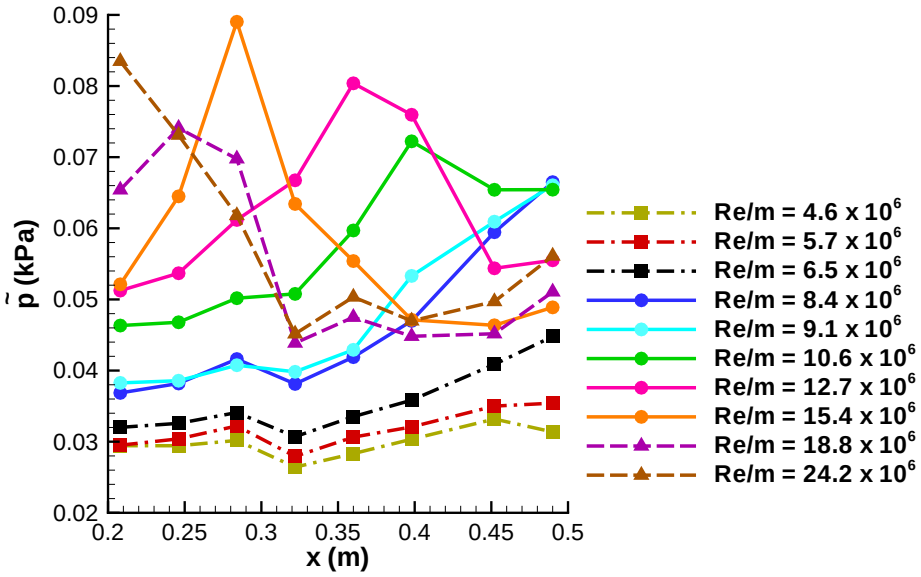

Figure 8. Unnormalized rms pressure along sharp cone in HWT-5

2. Normalization of Pressure Fluctuations

The magnitude of the unnormalized pressure fluctuations increases with Re/m. A normalization of the fluctuations is desired to collapse data at different freestream conditions. Various parameters have been used in the literature for normalization of pressure fluctuations. The most common are p_e and q_e. τ_w has also been used since this parameter is an important factor for tunnel noise generation. Raman[5] and Laderman[10] reviewed various normalizing parameters for freestream tunnel noise and found that the nozzle wall shear stress worked the best. If the laminar or turbulent pressure fluctuations are a reflection of tunnel noise, then the nozzle wall shear stress should collapse the pressure fluctuations on the cone.

Figures 9(a) through 9(c) show the rms pressure fluctuation in HWT-5 normalized by p_e, q_e, and τ_w, respectively. Laminar fluctuations are seen in the first three sensors below $Re/m = 12.7 \times 10^6$. Both p_e and q_e collapse the laminar fluctuations somewhat, however, there is still scatter. τ_w collapses the laminar fluctuations much better, in agreement with Raman and Laderman's results. This collapse with τ_w is an indication that the laminar pressure fluctuations are in fact a reflection of tunnel noise. The fluctuations following transition fall back towards the laminar level. This seems counter-intuitive, but is likely the result of high levels of tunnel noise; experiments have shown that turbulent boundary layers can attenuate tunnel noise.[14] Similar results were obtained in both the BAM6QT and in HWT-8 and are discussed in Reference 31.

D. Power Spectral Density During Boundary-Layer Transition

Power spectral densities (PSD) were calculated for the Kulite data to show the changing frequency contributions to the rms pressure during transition. The pressure was normalized by p_e to show the strength of the fluctuations relative to the mean. Kulite spectra were calculated for 0.1 s time samples using Welch's method. A Blackman window was used with a window size of 410 points and a 25% overlap. Approximately 976 FFT's were averaged.

A typical PSD during transition is shown in Figure 10. The first sensor at x = 0.208 m is under a laminar boundary layer. There is still a high level of broadband fluctuations under the laminar boundary layer because of the tunnel noise. The next two sensors (at x = 0.246 and 0.284 m) show the onset of transition. There is first an increase in frequency components above 20 kHz, shown by the second sensor. The third sensor

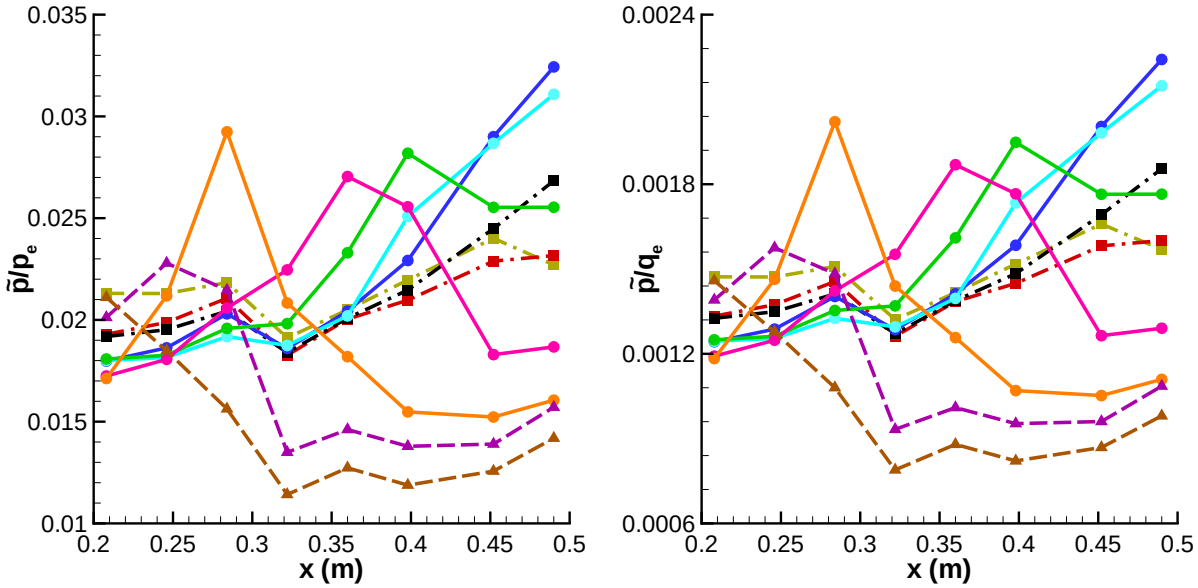

(a)

(b)

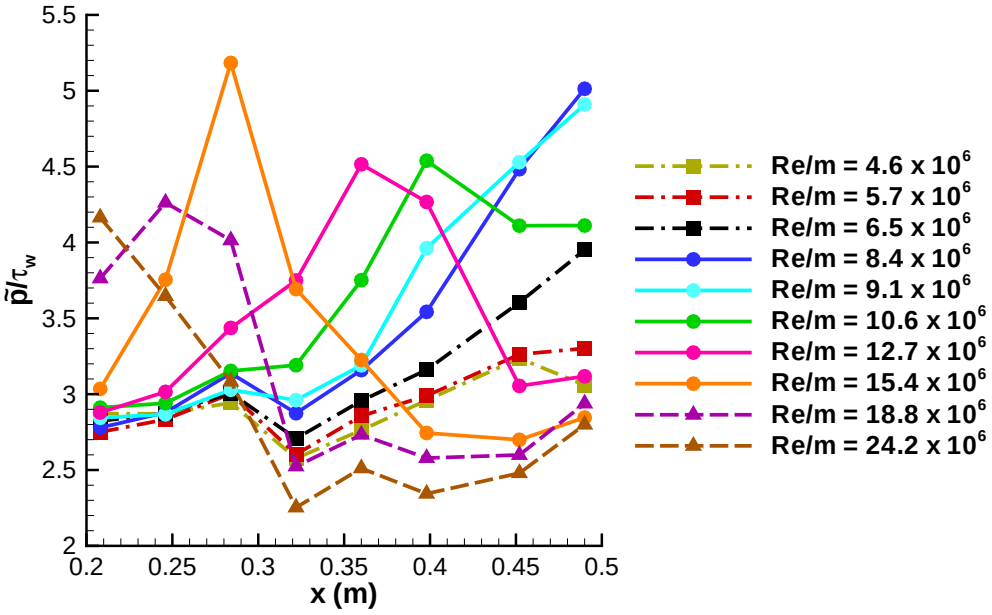

(c)

Figure 9. Normalized rms pressure along sharp cone in HWT-5 (a) Edge pressure; (b) Edge dynamic pressure; (c) Nozzle wall shear stress

shows an increase in frequency components above 15 kHz as well as a rise in lower frequencies. As transition progresses, the rms fluctuations peak. This peak is marked by a large increase in frequencies below 15 kHz. After the transitional peak, the spectrum drops back towards the laminar level. It seems counter-intuitive that the turbulent level is similar to the laminar level, but this may be due to tunnel noise.[14] This same trend was also seen in the BAM6QT and in HWT-8.[31] However, both tunnels (particularly in HWT-8) have higher noise levels which disguise the trends seen in HWT-5.

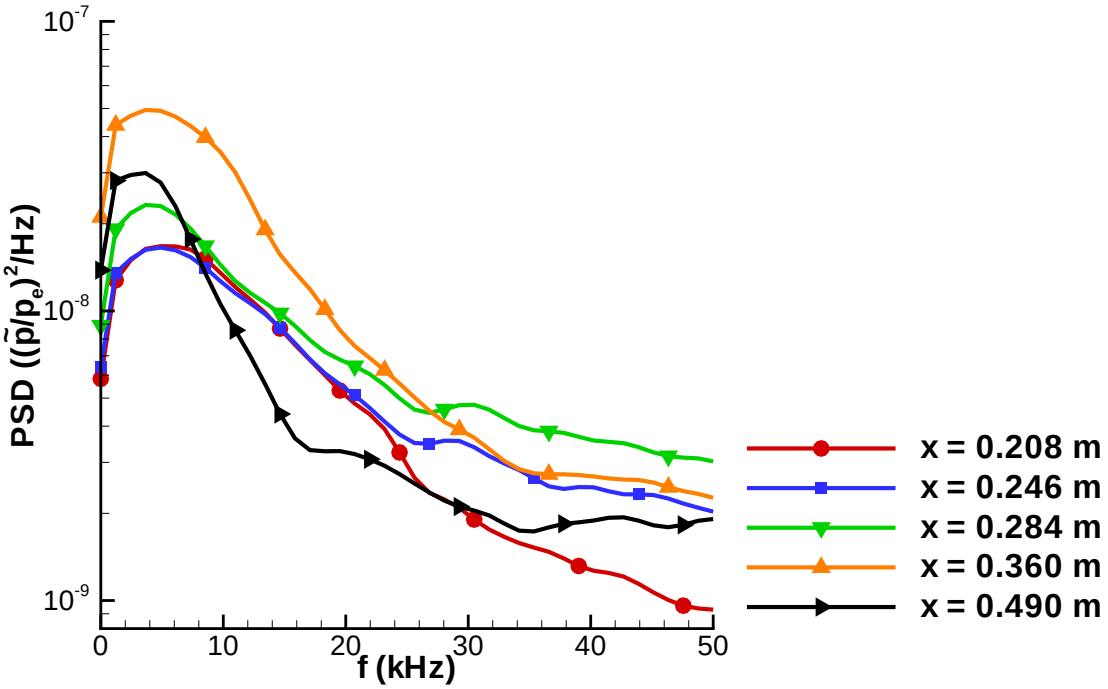

Figure 10. Transitional power spectral densities for pressure fluctuations normalized by edge pressure along sharp cone (HWT-5, $Re/m = 12.7 \times 10^6$)

E. Pressure Fluctuation Variation with Freestream Reynolds Number

In an effort to understand how tunnel noise affected the measured pressure fluctuations, freestream Pitot probe measurements of tunnel noise were conducted in HWT-5 and HWT-8. Measurements were made with an XCQ-062-25A B-screen sensor mounted in a centerline Pitot probe at the same axial location as the cone nosetip. Pressure fluctuations normalized by p_e along the cone were replotted against freestream unit Reynolds number (Figure 11). This allows a direct comparison to the tunnel noise measurements. The laminar pressure fluctuations on the cone agree well with the freestream noise level measured by the Pitot probe when normalized by the mean Pitot pressure. Laminar fluctuations are initially close to the tunnel noise level but deviate slightly above the noise level further downstream. However, there is no significant amplification of the freestream noise in the laminar boundary layer. As transition progresses, the pressure fluctuations rise above the noise level and peak near the end of transition. Once the flow is late transitional or turbulent, the pressure fluctuations fall back towards the freestream noise level. Normalizing by τ_w (not shown) flattens the variation of maximum fluctuation amplitudes with Re/m.[31] These results were consistent in both the BAM6QT and in HWT-8.

F. Pate's Correlation for Transition on Models in Noisy Tunnels

Pate conducted extensive research into transition in several different conventional hypersonic wind tunnels in the 1970's.[28] He was able to show that tunnel noise dominates the transition process for flat plates and sharp cones at zero angle of attack. This had been suspected in previous work by Laufer[41] and others. Pate developed a correlation to predict the transition location on flat plates and sharp cones at zero incidence based on tunnel noise parameters: the tunnel wall turbulent boundary layer mean parameters ($C_{F_{II}}$ and

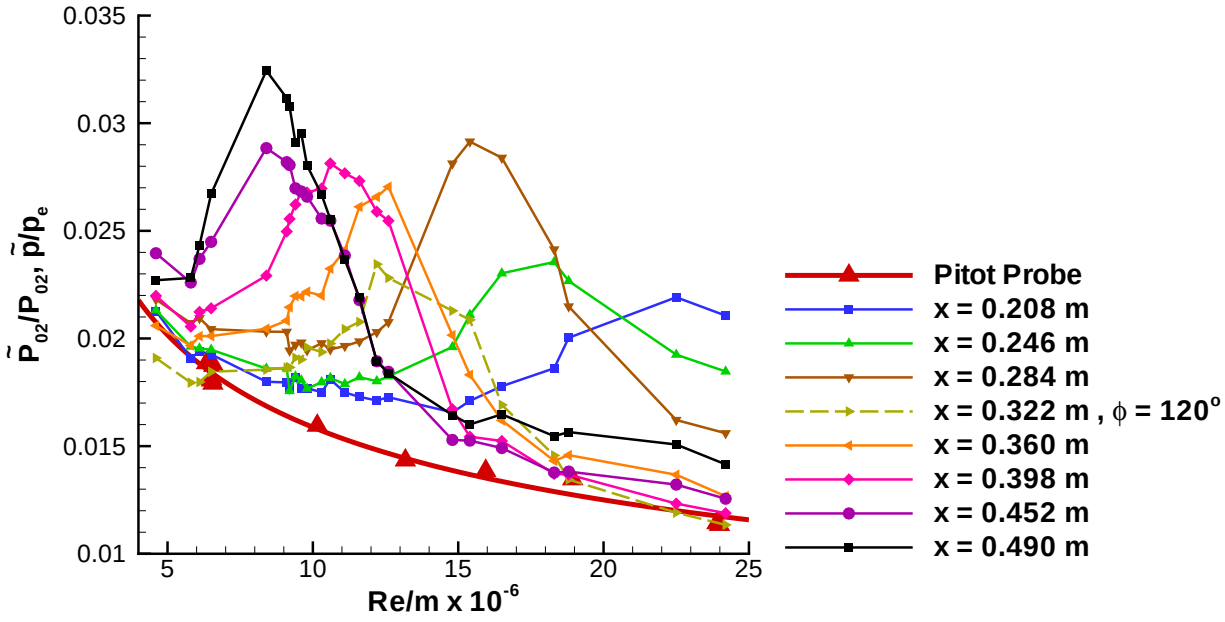

Figure 11. HWT-5 pressure fluctuations normalized by edge pressure as a function of freestream unit Reynolds number

δ^*) and the test section circumference (c). The correlation for sharp slender cones (Equation 1) gives the transition location, defined as the end of transition corresponding to the peak rms in surface Pitot probe measurements. The test section circumference of a 0.305 × 0.305 m tunnel is given by c_1.

$$
\begin{aligned}
&[(\mathrm{Re}_t)_\delta]_{cone} = \frac{(C_{F_{II}})^{-1.40}(\bar{c})}{\left[\frac{\delta^*}{c}\right]^{\frac{1}{2}}} \\
&\bar{c} = 0.8 + 0.2\left(\tfrac{c_1}{c}\right) \; for \; \tfrac{c_1}{c} < 1.0 \\
&\bar{c} = 1.0 \; for \; \tfrac{c_1}{c} > 1.0
\end{aligned}
\tag{1}
$$

The measured transition location varies based on which transition detection method is used. To compare transition measurements obtained with different transition detection methods, Pate correlated different methods to the corresponding location measured by surface Pitot probes (Pate's primary means of transition detection). This correlation was extrapolated to higher Mach numbers and used to compare surface pressure fluctuations from the present work to Pate's transition location correlation. The resulting transition location compared to sharp cone data from HWT-5 can be seen in Figure 12. The transition location given by Pate's correlation is shown by the vertical lines. There is fair agreement between experiments and the correlation. The expected trend for movement of transition with increasing Re/m can be seen. However, the correlation predicts transition after the peak fluctuations at higher Re/m and before the peak at lower Re/m for unknown reasons. Consistent results were obtained in both the BAM6QT and HWT-8.[31]

G. Comparison of Pressure Fluctuations under Noisy and Quiet Flow in the BAM6QT

Because the BAM6QT can run with either noisy or quiet flow, the tunnel provides a unique environment to directly show tunnel noise effects on the measured fluctuations. The cone was run under quiet-flow conditions that matched noisy-flow freestream Reynolds numbers. The Mach number under quiet flow is higher than noisy flow because the laminar boundary layer is thinner: $M = 6$ under quiet flow while $M = 5.8$ for noisy-flow runs. As a result, conditions are not exactly matched between quiet and noisy runs.

In all quiet-flow cases, the flow remained laminar over the entire cone, even when transition occurred well forward on the model under noisy flow. Figure 13(a) shows a comparison between noisy and quiet-flow runs at similar Re/m. The background noise with no tunnel flow is also shown. The first sensor at x= 0.208 m is seeing the onset of transition under noisy flow and transition occurs downstream. The pressure fluctuations are almost an order of magnitude lower under quiet flow. Figure 13(b) show the PSD at x = 0.208 m for

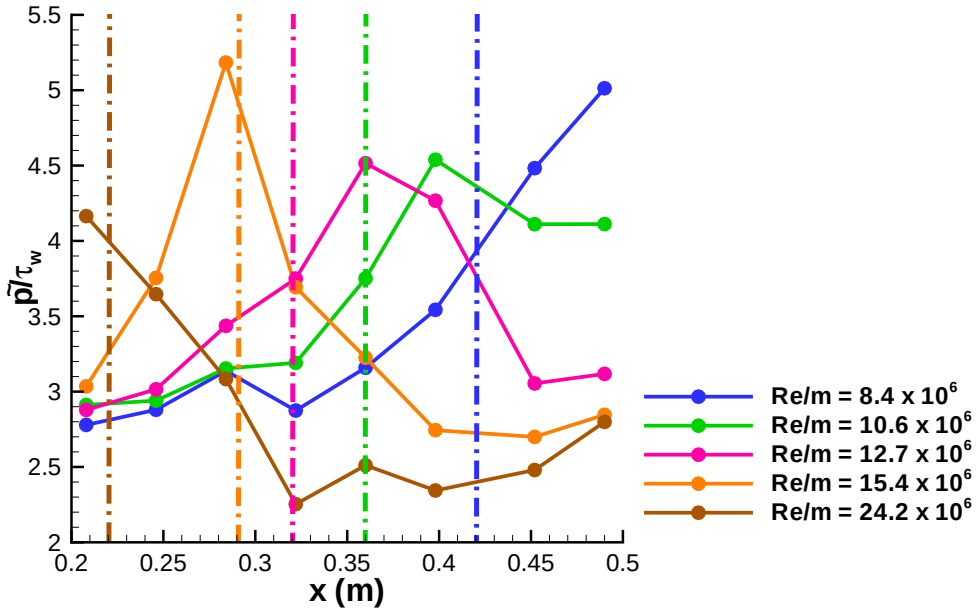

Figure 12. Predicted transition location from Pate's correlation (vertical lines) compared to HWT-5 measurements

these runs in the BAM6QT. The noisy-flow spectrum is higher across all frequencies than for quiet flow, though the quiet-flow spectrum shows some low-frequency content.

H. Measurements of Second-Mode Waves

Second-mode waves are the dominant instability on cones at zero angle of attack for hypersonic edge Mach numbers.[42] The waves are like trapped acoustic waves that reflect between the wall and the edge of the boundary layer. Initially, the unstable waves grow linearly. Prior to transition, the waves become nonlinear and then break down to turbulence. This breakdown should correspond to the point where turbulent spots begin to appear. Flow intermittency develops and increases until the flow eventually becomes fully turbulent.

Second-mode waves were measured with three PCB132 sensors at positions 1B, 5B, and 8B. Power spectral densities were calculated for 0.1 s samples using Welch's method. A Blackman window was used with a window size of 1024 points for HWT data and 2048 points for the BAM6QT. A 25% overlap was used and approximately 976 FFT's were averaged for both cases. To compare second-mode wave strength prior to breakdown in each tunnel, the normalized power density $((\tilde{p}/p_e)^2/Hz)$ at the most amplified frequency is used. Second-mode wave rms amplitudes are also compared. The power of the waves was obtained by integrating the unnormalized PSD over the amplified frequency band. Taking the square root of the power ($\times 100$) and then normalizing by p_e gives the rms amplitude of the waves as a percentage of the edge pressure.

1. HWT-5

Figure 14(a) shows PCB132 power spectral densities for $Re/m = 9.1 \times 10^6$. The Kulite pressure fluctuations indicate peak pressure fluctuations at the rear of the cone (Figure 9(a)) for this run. The first PCB132 at x = 0.208 m shows no indication of second-mode waves. This sensor also shows higher electrical noise than the other two sensors for unknown reasons. The second PCB132 at x = 0.360 m shows a second-mode wave with a peak frequency near 280 kHz. A smaller secondary peak is also evident near 670 kHz. This location on the cone corresponds to the beginning of the rise in Kulite pressure fluctuations. The third PCB132 (x = 0.490 m) is at the rear of the cone where the peak in Kulite fluctuations is seen. The second-mode waves have broken down and are no longer visible. However, the broadband frequency spectrum is higher and significant frequency content is seen up to 650 kHz.

The second-mode waves were small in HWT-5. Figure 14(b) shows a wave at x = 0.490 m on the cone as it grows and then breaks down with increasing Reynolds number. The normalized power density of the most

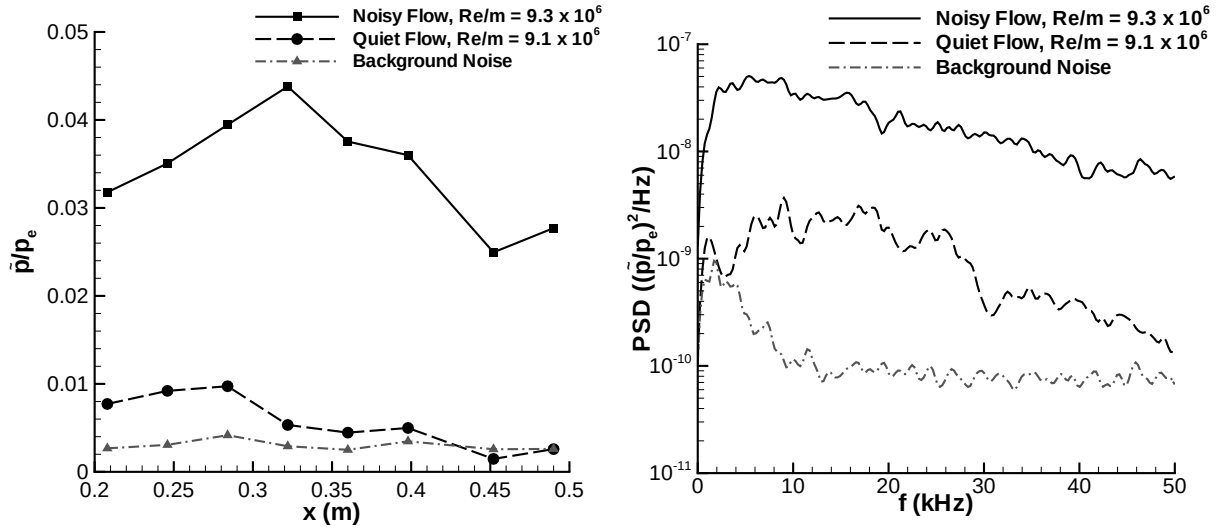

(a) (b)

Figure 13. Comparison of pressure fluctuations under noisy and quiet flow (BAM6QT, Mic-062 A-screens) (a) RMS pressure normalized by edge pressure; (b) PSD normalized by edge pressure (x = 0.208 m)

amplified frequency is $2.6 \times 10^{-8}/Hz$, and the rms amplitude of the second-mode waves is approximately 1.7% before breakdown. This small amplitude is probably because of the low edge Mach number of 4.6 in HWT-5. Second-mode waves typically grow only at hypersonic edge Mach numbers. Waves in the BAM6QT and HWT-8 are much larger, as seen below.

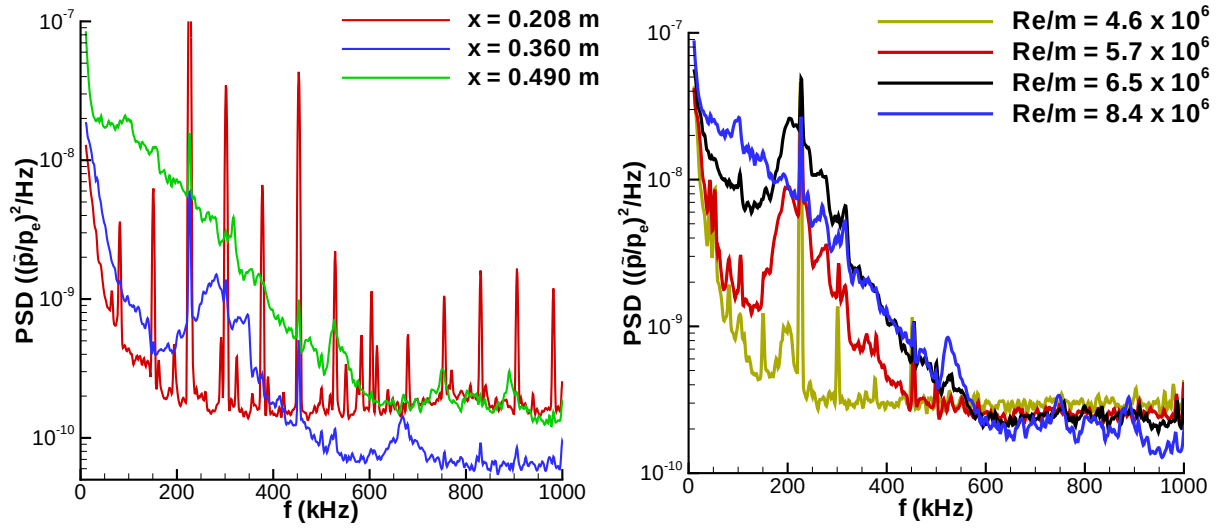

(a) (b)

Figure 14. PCB132 power spectral densities showing second-mode waves in HWT 5 (a) Transitional spectra ($Re/m = 9.1 \times 10^6$); (b) Second-mode wave growth and breakdown (x = 0.490 m)

2. BAM6QT Noisy-Flow Measurements

Second-mode waves were also seen in the BAM6QT. Figure 15(a) shows the results for a noisy run with transition over the middle portion of the cone. At x = 0.208 m, a small second-mode wave can be seen centered at 275 kHz. The flow here is still laminar as defined by the Kulite fluctuations (Figure 15(b)). By x = 0.360 m, the second-mode wave has grown in amplitude and decreased in frequency to 205 kHz. A likely

harmonic of the wave can also be seen at 410 kHz and there is an increase in broadband frequency content. The Kulite pressure fluctuations indicate transition onset near this location. Rufer[38] measured second-mode waves at 200 kHz with hot wires at this location and at similar freestream conditions. Robarge[43] performed a stability analysis for these conditions and computed a peak second-mode frequency of 200 kHz and an N factor of 4.7. Between x = 0.360 and 0.452 m, the Kulite fluctuations peak, indicating the end of transition. Breakdown of the second-mode waves is complete by x = 0.490 m and broadband high-frequencies remain.

The second-mode waves in the BAM6QT have larger amplitudes than in HWT-5. Figure 15(c) shows PCB132 spectra at x = 0.360 m for increasing Re/m. A small second-mode wave can be seen at 160 kHz. As the Re/m increases, the wave grows in amplitude. The wave also shifts to higher frequencies as the boundary layer thins, and a harmonic of the wave becomes visible. At $Re/m = 8.5 \times 10^6$ the wave begins to break down, and breakdown is complete by $Re/m = 10.0 \times 10^6$. The rms amplitude of the second-mode waves before breakdown is approximately 4.3%, and the normalized power density of the most amplified frequency is $3.0 \times 10^{-7}/Hz$. This is larger than the waves seen in HWT-5 but smaller than those in HWT-8.

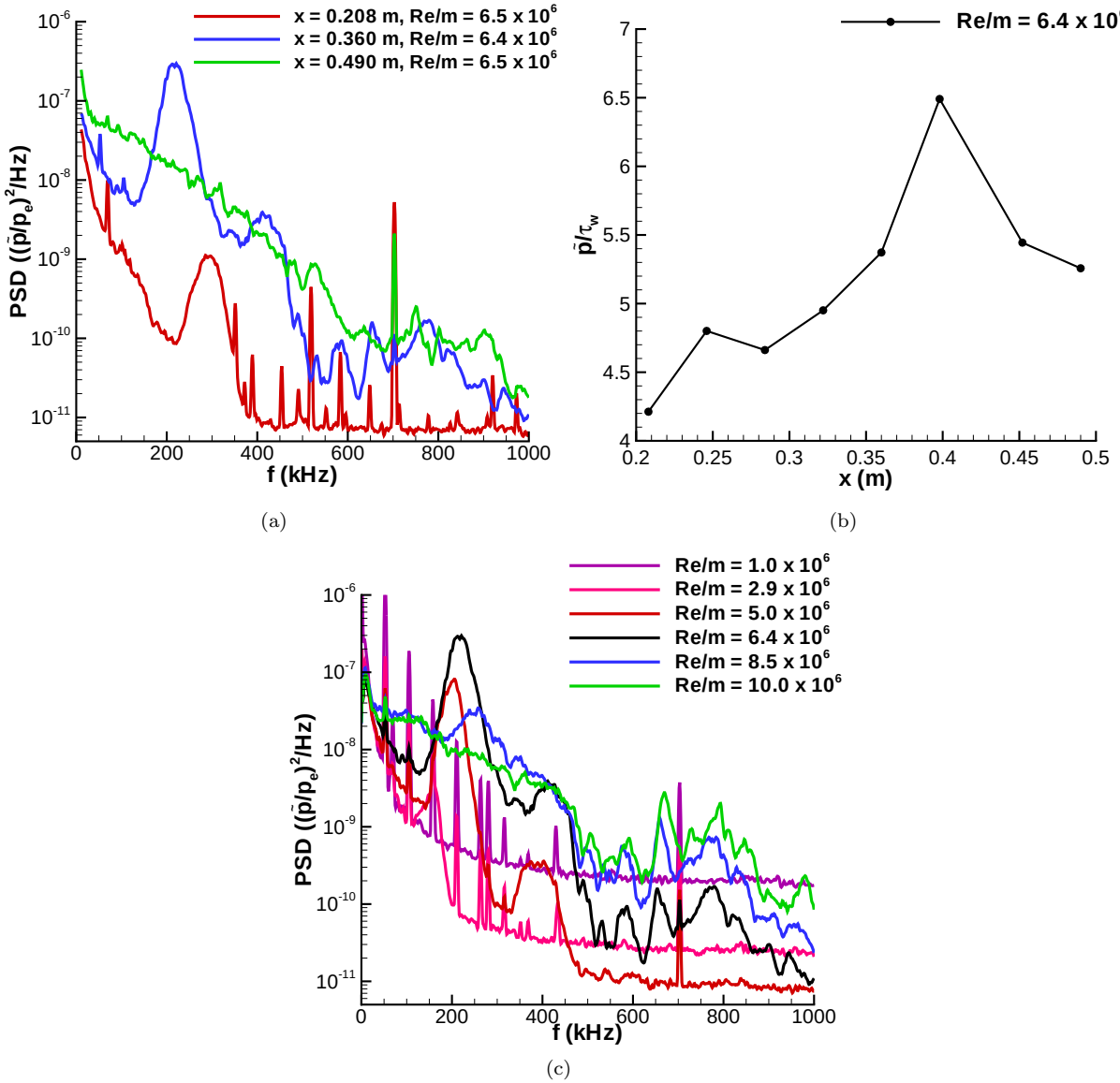

Figure 15. PCB132 power spectral densities showing second-mode waves in the BAM6QT (noisy flow) (a) Transitional spectra; (b) Mic-062 A-screen rms pressure fluctuations normalized by p_e along cone; (c) Second-mode wave growth and breakdown (x = 0.360 m)

3. *BAM6QT Quiet-Flow Measurements*

Measurements were repeated under quiet flow. Figure 16 shows a comparison of waves measured under quiet flow compared to noisy-flow results. Second-mode waves can be seen at 220 and 235 kHz under quiet flow. The rms amplitude of the quiet-flow waves is approximately 0.13%, more than an order of magnitude lower than under noisy flow. Under noisy flow, the waves are centered at 330 and 350 kHz and the rms amplitude of the waves is 2.1%. However, these waves cannot be directly compared. Under quiet flow, the waves are only seen at the last sensor location (x = 0.490 m). The noisy-flow waves appear at the first sensor location (x = 0.208 m) and have broken down by the end of the cone. Further normalization using the edge velocity and the boundary-layer thickness should allow a more direct comparison.

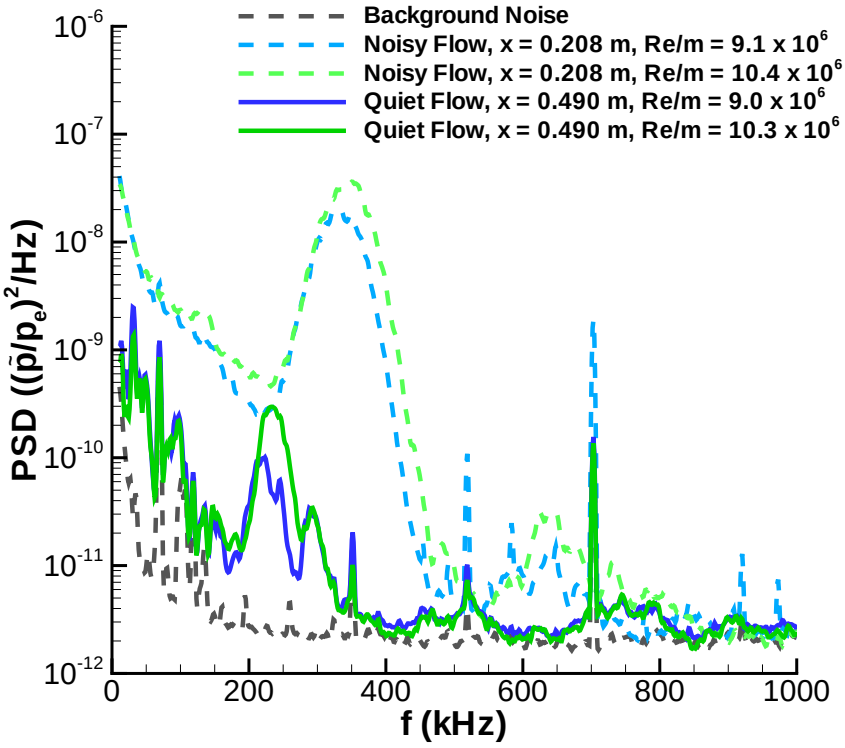

Figure 16. PCB132 power spectral densities showing second-mode waves under noisy and quiet flow (BAM6QT)

4. *HWT-8*

Second-mode waves were largest in HWT-8. This is expected because the edge Mach number is 6.8, higher than in the other tunnels. Figure 17(a) shows PCB132 power spectral densities along the cone for a nominally laminar case. Large second-mode waves are seen at all sensor locations. At x = 0.208 m, a small wave is centered at 295 kHz. By x = 0.360 m, the second-mode wave has grown significantly. The peak frequency of the wave has also decreased to 220 kHz because of the thickening of the boundary layer. Two harmonics appear near 415 kHz and 670 kHz. The third sensor at x = 0.360 m shows an even larger second-mode wave at 180 kHz. The harmonics have also grown in power and decreased in frequency to 350 and 525 kHz, respectively. Despite the presence of the large waves and harmonics, breakdown does not occur and the boundary layer remains laminar as defined by Kulite pressure fluctuations along the cone (Figure 17(c)).

Figure 17(b) shows a higher Re/m case where transition occurs over the middle portion of the cone. The first sensor is under fully laminar flow. A large-amplitude second-mode wave at 320 kHz as well as a harmonic at 615 kHz can be seen. The second sensor at x = 0.360 m is in the middle of the peak fluctuations seen by the Kulite sensors (Figure 17(c)). In this case, the second-mode wave near 230 kHz has started to break down but is still visible. Higher frequency broadband components are seen throughout the spectrum. The third sensor at x = 0.490 m corresponds to turbulent flow as indicated by Kulite fluctuations. The

second-mode waves are no longer visible on the cone, and there are now broadband frequency components.

Figure 17(d) shows PCB132 spectra at x = 0.360 m for increasing Re/m. Similar growth and breakdown to turbulence as in HWT-5 and the BAM6QT are seen. The rms amplitude of the second-mode waves is approximately 8.9% before breakdown, and the normalized power density of the most amplified frequency is $1.1 \times 10^{-6}/Hz$, higher than in both HWT-5 and the BAM6QT. Comparisons of these second-mode wave measurements to computations are forthcoming.

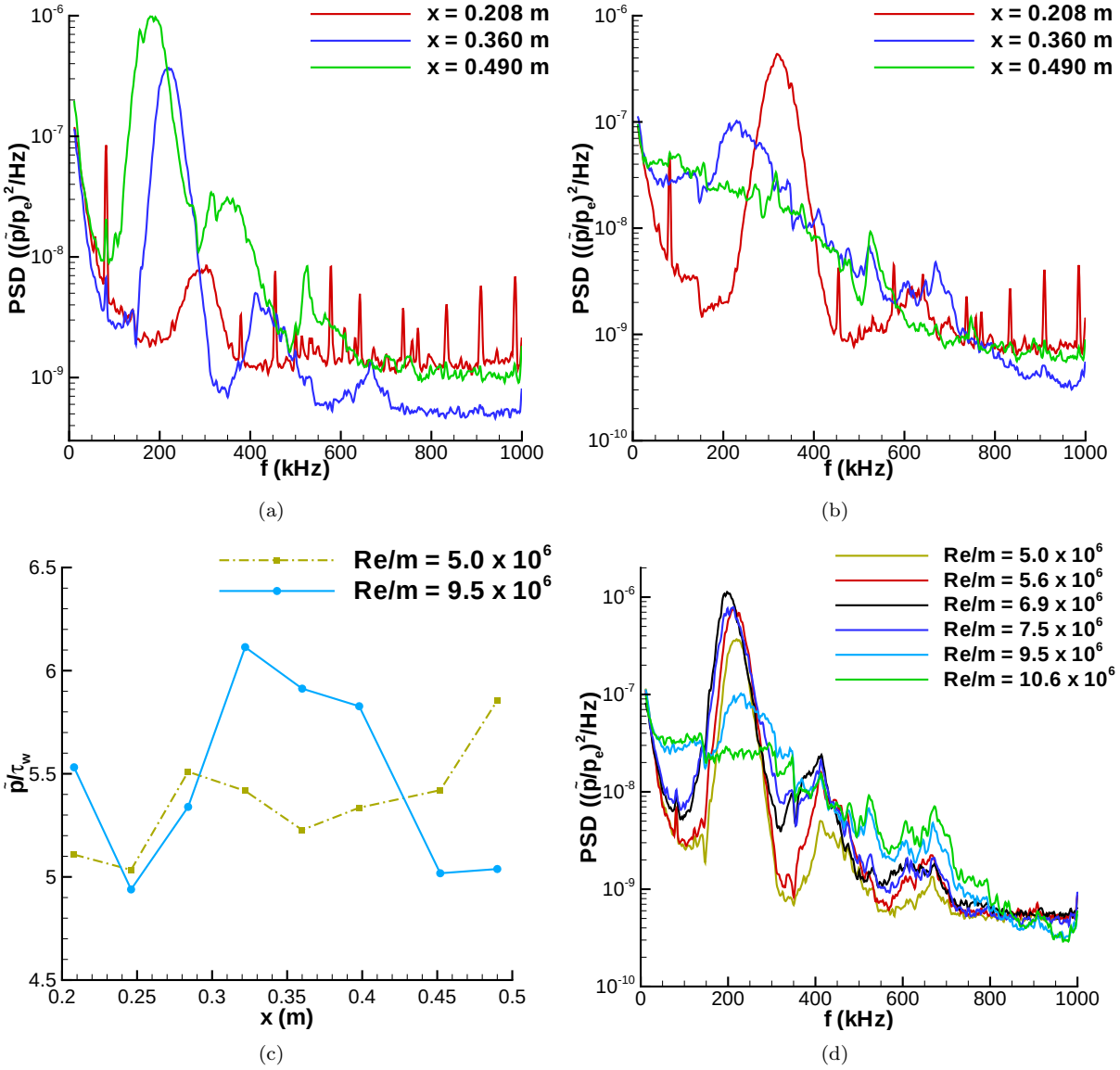

Figure 17. PCB132 power spectral densities showing second-mode waves in HWT-8 (a) Laminar spectra, $Re/m = 5.0 \times 10^6$; (b) Transitional spectra, $Re/m = 9.5 \times 10^6$; (c) Mic-062 A-screen rms pressure fluctuations normalized by p_e along cone; (d) Second-mode wave growth and breakdown (x = 0.360 m)

I. Measurement Uncertainty

There are many possible sources of measurement error including flow nonuniformity and model imperfection effects. Both can affect the pressure fluctuations as well as transition symmetry. Other possible sources include sensor and insert mounting, sensor bias error, spatial resolution, sensor resonance and frequency response, and electrical noise. To investigate flow axisymmetry and repeatability, runs were repeated in HWT-5 and 8 by pitching the model up and down by 0.1 degrees and also rolling the cone. Also, because no

sharp nosetip is truly sharp, repeat runs with both nosetips were conducted. The percent difference in laminar fluctuation measurements are small; the typical difference between runs was 2–3%, with a maximum of approximately 6%. Transitional measurements are more sensitive to tiny changes; a small motion of transition location relative to the sensors can appear as a large change in the measured fluctuations. Differences in transitional pressure fluctuations were often as low as 2–3% but typically around 8–10%. However, some differences as high as 20% were observed. When comparing separate runs, there is also a scatter in the freestream conditions which can contribute to the observed scatter in results. Although these runs help define the precision of the data, bias errors cannot be traced in this manner. Dynamic calibrations of the sensors will help address the accuracy of the measurements. A complete uncertainty investigation is beyond the scope of the present document, but will see future attention.

VI. Concluding Remarks

Measurements of pressure fluctuations on a 7° sharp cone were conducted in Sandia's Hypersonic Wind Tunnel at Mach 5 and 8. Tests were also conducted in Purdue University's Boeing/AFOSR Mach-6 Quiet Tunnel under noisy and quiet flow.

Sensor comparisons of Mic-062 A-screens, XCQ-062 B-screens and PCB132's were conducted under a laminar boundary layer. The Kulite A-screen sensors were found to work best for dynamic measurements below 50 kHz. B-screen sensors rolled off at lower frequencies than the A-screens. PCB132 sensors offered an independent measurement; they could be used for comparison to Kulites between 11 and 50 kHz as well as for higher frequency measurements up to 1 MHz. Good agreement between the Mic-062 A-screens and PCB132's in the overlap region between 11 and 50 kHz was found under laminar boundary layers. Responses under transitional/turbulent boundary layers were higher in the PCB132's.

Pressure fluctuations were measured along the cone at different freestream Reynolds numbers. Mic-062 A-screens showed a peak in the pressure fluctuations during transition. This peak showed fair agreement with transition location predictions using Pate's correlation. To investigate tunnel noise effects, freestream noise measurements were made in HWT-5 and 8. Noise levels were reflected in the laminar pressure fluctuations. Fluctuations following transition also approached the tunnel noise level. Quiet-flow measurements confirmed that the laminar pressure fluctuations are primarily due to tunnel noise and that tunnel noise causes early model transition. Transition did not occur on the model under quiet flow.

Second-mode waves were measured in all tunnels. The initial growth of the second mode waves was seen under a laminar boundary layer. The sensors showed wave breakdown near the peak transitional pressure fluctuations measured by Kulites. The maximum observed rms amplitude of the second-mode waves prior to breakdown was 1.7% in HWT-5, 4.3% in the BAM6QT under noisy flow, and up to 8.9% in HWT-8. After breakdown, the PCB132's showed broadband spectra components up to very high frequency. Small second-mode waves up to 0.13% were measured under quiet flow in the BAM6QT, but did not break down.

Transitional measurements could only be made under noisy flow because the model boundary layer remained laminar under quiet flow in the BAM6QT. However, both noisy and quiet-flow measurements showed the growth of the second-mode instability. Because of the similar growth of instabilities, further study of noisy-flow measurements should help understand the physics behind transition as well as the generation of boundary layer pressure fluctuations.

Acknowledgments

This work could not have been completed without the help of many individuals. The Purdue Ludwieg Tube Group (particularly Matt Borg, Tom Juliano, and Brad Wheaton) provided advice and suggestions throughout the project. Tom Grasser, Roger Harmon, and the Purdue Aerospace Sciences Laboratory machine shop contributed greatly to the model design. This work was funded in part by the National Defense Science and Engineering Graduate Fellowship, Sandia National Laboratories, and AFOSR.

References

[1]Houbolt, J., "On the Estimation of Pressure Fluctuations in Boundary Layers and Wakes," GE TIS66SD296, April 1966.
[2]Lowson, M., "Prediction of Boundary Layer Pressure Fluctuations," AFFDL-TR-67-167, April 1968.
[3]Martellucci, A., Chaump, L., Rogers, D., and Smith, D., "Experimental Determination of the Aeroacoustic Environment

about a Slender Cone," *AIAA Journal*, Vol. 11, No. 5, 1973, pp. 635–642.

[4]Chaump, L., Martellucci, A., and Monfort, A., "Aeroacoustic Loads Associated with High Beta Re-entry Vehicles," Tech. Rep. TR-72-138, AFFDL, May 1973, Volume I.

[5]Raman, K., "Surface Pressure Fluctuations in Hypersonic Turbulent Boundary Layers," AIAA Paper 73-997, October 1973.

[6]Laganelli, A. L., Martellucci, A., and Shaw, L., "Prediction of Surface Pressure Fluctuations in Hypersonic Turbulent Boundary Layers," AIAA Paper 76-409, July 1976.

[7]Laganelli, A. L., and Howe, J., "Prediction of Pressure Fluctuations Associated with Maneuvering Reentry Vehicles," AFFDL-TR-77-59, July 1977.

[8]Laganelli, A., Martellucci, A., and Shaw, L., "Prediction of Turbulent Wall Pressure Fluctuations in Attached Boundary Layer Flow," AIAA Paper 81-1227, June 1981.

[9]Laufer, J., "Some Statistical Properties of the Pressure Field Radiated by a Turbulent Boundary Layer," *The Physics of Fluids*, Vol. 7, No. 8, 1964, pp. 1191–1197.

[10]Laderman, A., "Review of Wind-Tunnel Freestream Pressure Fluctuations," *AIAA Journal*, Vol. 15, No. 4, 1977, pp. 605–608.

[11]Beckwith, I. E., and Miller III, C., "Aerothermodynamics and Transition in High-Speed Wind Tunnels at NASA Langley," *Annual Review of Fluid Mechanics*, Vol. 22, 1991, pp. 419–439.

[12]Schneider, S. P., "Effects of High-Speed Tunnel Noise on Laminar-Turbulent Transition," *Journal of Spacecraft and Rockets*, Vol. 38, No. 3, 2001, pp. 323–333.

[13]Schneider, S. P., "Flight Data for Boundary-Layer Transition at Hypersonic and Supersonic Speeds," *Journal of Spacecraft and Rockets*, Vol. 36, No. 1, 1999, pp. 8–20.

[14]Beckwith, I. E., "Development of a High Reynolds Number Quiet Tunnel for Transition Research," *AIAA Journal*, Vol. 13, No. 3, 1975, pp. 300–306.

[15]Schneider, S. P., "The Development of Hypersonic Quiet Tunnels," *Journal of Spacecraft and Rockets*, Vol. 45, No. 4, 2008, pp. 641–664.

[16]Stainback, P. C., "Hypersonic Boundary-Layer Transition in the Presence of Wind-Tunnel Noise," *AIAA Journal*, Vol. 9, No. 12, 1971, pp. 2475–2476.

[17]Stainback, P. C., Fischer, M., and Wagner, R., "Effects of Wind-Tunnel Disturbances on Hypersonic Boundary-Layer Transition," AIAA Paper 72-181, January 1972.

[18]Owen, F., Horstman, C., Stainback, P. C., and Wagner, R., "Comparison of Wind Tunnel Transition and Freestream Disturbance Measurements," *AIAA Journal*, Vol. 13, No. 3, 1975, pp. 266–269.

[19]Stainback, P. C., and Rainey, R., "Correlation of Freestream Pressure Disturbances in Supersonic Wind Tunnels," *AIAA Journal*, Vol. 14, No. 2, 1976, pp. 286–288.

[20]Kendall, J., "Wind Tunnel Experiments Relating to Supersonic and Hypersonic Boundary-Layer Transition," *AIAA Journal*, Vol. 13, No. 3, 1975, pp. 290–299.

[21]Pate, S. R., "Effects of Wind-Tunnel Disturbances on Boundary-Layer Transition with Emphasis on Radiated Noise: A Review," AIAA Paper 1980-0431, March 1980.

[22]Mack, L. M., "Linear Stability Theory and the Problem of Supersonic Boundary-Layer Transition," *AIAA Journal*, Vol. 13, No. 3, 1975, pp. 278–289.

[23]Schopper, M. R., "Interaction of Aerodynamic Noise with Laminar Boundary Layers in Supersonic Wind Tunnels," Tech. Rep. 3621, NASA Contractor Report, April 1984.

[24]Fischer, M., and Weinstein, L., "Cone Transitional Boundary-Layer Structure at $M_e = 14$," *AIAA Journal*, Vol. 10, No. 5, 1972, pp. 699–701.

[25]Pate, S., and Brown, M., "Acoustic Measurements in Supersonic Transitional Boundary Layers," Tech. Rep. AEDC-TR-69-182, Arnold Engineering Development Center, October 1969.

[26]Johnson, R. I., Macourek, M. N., and Saunders, H., "Boundary Layer Acoustic Measurements in Transitional and Turbulent Flow at $M_\infty = 4.0$," AIAA Paper 69-344, April 1969.

[27]Cassanto, J., and Rogers, D., "An Experiment to Determine Nose Tip Transition with Fluctuating Pressure Measurements," *AIAA Journal*, Vol. 13, No. 10, October 1975, pp. 1257–1258.

[28]Pate, S. R., "Dominance of Radiated Aerodynamic Noise on Boundary-Layer Transition in Supersonic/Hypersonic Wind Tunnels," Tech. Rep. AEDC-TR-77-107, Arnold Engineering Development Center, March 1978.

[29]Owen, F., and Horstman, C., "Hypersonic Transitional Boundary Layers," *AIAA Journal*, Vol. 10, No. 6, 1972, pp. 769–775.

[30]Juliano, T., Schneider, S., Aradrag, S., and Knight, D., "Quiet-Flow Ludwieg Tube for Hypersonic Transition Research," *AIAA Journal*, Vol. 46, No. 7, 2008, pp. 1757–1763.

[31]Casper, K. M., *Hypersonic Wind-Tunnel Measurements of Boundary-Layer Pressure Fluctuations*, Master's Thesis, Purdue University School of Aeronautics & Astronautics, To appear August 2009.

[32]Fujii, K., "Experiment of Two Dimensional Roughness Effect on Hypersonic Boundary-Layer Transition," *Journal of Spacecraft and Rockets*, Vol. 43, No. 4, 2006, pp. 731–738.

[33]Estorf, M., Radespiel, R., Schneider, S. P., Johnson, H., and Hein, S., "Surface-Pressure Measurements of Second-Mode Instability in Quiet Hypersonic Flow," AIAA Paper 2008-1153, January 2008.

[34]Stetson, K., Kimmel, R., Thompson, E., Donaldson, J., and Siler, L., "A Comparison of Planar and Conical Boundary Layer Stability at a Mach Number of 8," AIAA Paper 91-1639, June 1991.

[35]Stetson, K. F., and Kimmel, R. L., "Example of Second-Mode Instability Dominance at a Mach Number of 5.2," *AIAA Journal*, Vol. 30, No. 12, 1992, pp. 2974–2976.

[36]Kimmel, R., Demetriades, A., and Donaldson, J., "Space-time Correlation Measurements in a Hypersonic Transitional Boundary Layer," AIAA Paper 95-2292, June 1995.

[37]Rufer, S. J., and Schneider, S. P., "Hot-Wire Measurements of Instability Waves on a Blunt Cone at Mach 6," AIAA Paper 2005-5137, June 2005.

[38]Rufer, S. J., *Hot-wire Measurements of Instability Waves on Sharp and Blunt Cones at Mach 6*, Ph.D. Thesis, Purdue University School of Aeronautics & Astronautics, December 2005.

[39]Rufer, S. J., and Schneider, S. P., "Hot-Wire Measurements of Instability Waves on Cones at Mach 6," AIAA Paper 2006-3054, June 2006.

[40]Keyes, F., "A Summary of Viscosity and Heat-Conduction Data for He, A, H_2, O_2, CO, CO_2, H_2O, and Air," *Transactions of the ASME*, Vol. 73, 1951, pp. 589–596.

[41]Laufer, J., "Aerodynamic Noise in Supersonic Wind Tunnels," *Journal of the Aerospace Sciences*, Vol. 28, No. 9, 1961, pp. 685–692.

[42]Mack, L. M., "Boundary Layer Linear Stability Theory," *Report 709, Special Course on Stability and Transition of Laminar Flow*, AGARD, March 1984, pp. 1–81.

[43]Robarge, T. W., *Laminar Boundary-Layer Instabilities on Hypersonic Cones: Computations for Benchmark Experiments*, Master's Thesis, Purdue University School of Aeronautics & Astronautics, August 2005.